A SOLDER SELF-ASSEMBLED LARGE ANGULAR DISPLACEMENT TORSIONAL ELECTROSTATIC MICROMIRROR

Brian McCarthy, Victor M. Bright, and John A. Neff*

Department of Mechanical Engineering, *Department of Electrical Engineering
University of Colorado at Boulder, CO 80309-0427, USA

ABSTRACT

Solder self-assembled micromirrors have the advantages of rigid electrical and structural connections to the substrate as well as compact assembly mechanisms. In addition solder assembly allows a structure to be rotated to any angle desired. In this work, these advantages are used to produce a novel electrostatic micromirror that can stably rotate $\pm 10^{o}$ from its assembled position. The compact solder mechanism allows each of three mirror components to be assembled independently to individual angles. After assembly the design is statically tested and compared to both analytical and finite element (FE) model results.

INTRODUCTION

Solder self-assembly is a well established assembly mechanism for surface micromachined devices [1-4]. It has several advantages over other methods of creating electrostatic micromirrors with large, stable rotation ranges. It provides a compact assembly mechanism and significant assembly force as well as solid post-assembly electrical and mechanical connections. In this work, a proof of concept for a unique torsional micromirror, actuated by parallel-plate electrostatic forces, is modeled, fabricated, assembled, and tested.

Outside of solder assembly, several other techniques are used to create micromirrors with larger stable rotation ranges. Syms uses a process similar to the described solder assembly for a micromirror assembly in [5]. However, in that case a nonconductive photoresist is used, and the mirror is driven with a rotating comb-drive. Other assembly and actuation methods have also been demonstrated. Arrays of scratch-drive actuators (SDAs) are used to assemble mirrors and parallel-plate electrodes in [6-7]. Alternatively, substrate mounted comb-drives are used to drive assembled mirrors through hinge linkages in [8-9]. However, each of these alternative cases has disadvantages including hinge linkages and manual assembly. The hinges are poor electrical connections, lack structural rigidity, and see excessive wear during operation. Manual assembly is also a disadvantage as it is not reliable or manufacturable. The current design overcomes the above problems with three solder assembled parallel-plate electrodes in an arrangement that provides a large, stable rotation range and reasonable actuation voltage.

After identifying the desirable characteristics a solder assembled micromirror provides, a simple analytical model is used to determine appropriate electrode gap heights and flexure dimensions. The resulting design is then fabricated in the JDS Uniphase/Cronos Multi-User MEMS Processes (MUMPS®) [10] and assembled using a solder self-assembly process developed at the University of Colorado at Boulder [3]. Following assembly, static testing is done to determine the voltage/angle relationship, which is compared to both analytical and FE model results. The process is then repeated for a second-generation design that is revised based on an improved analytical model and experience with the assembly process.

DESIGN AND MODELING

While solder assembly can be used to rotate a structure to any desired angle, the micromirror presented here is constrained to a stable 20^{o} rotation range from 25^{o} – 45^{o} above the substrate. The most efficient way of accomplishing this is to use a mirror neutral position 35^{o} above the substrate and have it rotate $\pm 10^{o}$ from there. The basic design concept utilizing these constraints is shown in Figure 1. The concept consists of three basic components, each of which is assembled with its own solder ball. The mirror, flexures, and mirror frame comprise one component. The other two components are the lower electrodes used to rotate the mirror in the positive and negative directions from the neutral axis. These components are rotated to 25^{o} and 45^{o} as suggested by the analytical model.

The analytical model is developed based on a torque balance between the electrostatic force on the mirror and the restoring torque of the flexures. The improved version also includes vertical deflection of the flexures using a force balance between the electrostatic force and the restoring force of the bent flexures. The improvements are necessary due to significant flexure deflection during actuation.

The basis of the model is the torque balance

$$k_t \theta = \int x f_e(\theta, x) dx$$

where θ is the change in mirror angle between the neutral and rotated positions. k_t is the torsional spring constant and f_e is the electrostatic force per unit length. These terms can be described as

$$k_t = \frac{JG}{L}$$

$$f_e = \frac{\varepsilon_0 w V^2}{2(d\cos\theta - v + x\tan(\alpha - \theta))^2}$$

where J is the torsional inertia of the flexures, G is the shear modulus, L is the flexure length, ε_0 is the permitivity of free space, and w is the electrode width. V is the applied voltage, d is the initial gap height, v is the vertical flexure deflection at the mirror edge, and α is the initial angle between the mirror and electrode. Once the flexure's vertical deflection at the mirror is calculated using

$$v = \frac{\int f_e dx L^3}{24EI}$$

where E is Young's Modulus and I is the bending inertia of the beam cross-section, the voltage/angle relationship can be determined. The initial model neglects the vertical flexure deflection and thus predicts that lower voltages and smaller gap heights will allow the mirror to stably rotate 10°. The revised model provides more realistic results that are used in the second-generation mirror design.

In addition to providing flexure dimensions and gap heights, the model also shows that the initial angle between the mirror and electrodes influences the pull-in threshold. For a specific configuration, the model predicts that a mirror and electrodes that are initially parallel would require a 60μm gap and 271V to allow 10° of rotation before pull-in. However, fixing the initial electrode positions 10° away from the mirror allows the gap to be decreased to 40μm at the closest point while still allowing 10° of stable rotation. In the non-parallel case, 242V are needed to reach 10°.

The insight from the analytical model is put to use in the mirror design as shown in the Figure 1 schematic. There it can be seen that the lower electrodes are rotated to 25° and 45°, 10° away from the mirror's neutral position. This rotation allows the smaller initial gap to be used. The first-generation design concept has a 23μm initial electrode gap, rather than the 40μm suggested by the improved model, because it was created with the original analytical model. Coupled with 2μm wide Poly 2 flexures that are 255μm long the improved model predicts this mirror will stably rotate 8.7° with 85.9V. The second-generation design, however, is designed with the improved model. Thus the initial electrode gap increases to 40μm. Also, shorter 100μm flexures are used for robustness. For this mirror, the improved model predicts 10° of stable rotation using 242.8V. In both generations, the mirrors are 250μm on a side.

Following testing of the assembled devices, a FE model, developed using Coventor Inc.'s Coventorware™ software [11], helps to verify the analytical model results. Although created and analyzed in Coventorware™, the model is meshed in I-DEAS®, from EDS [12], due to the non-parallel nature of the electrodes. This necessitates some simplifications, such as eliminating multi-layer sections and surface irregularities associated with conformally deposited layers. Once meshed, the model is imported back into Coventorware™ where the pull-in analysis is performed with the CosolveEM electro-mechanical solver module. The analysis, performed on the second-generation mirror, predicts a pull-in at 10.8° and 238.8V.

FABRICATION, ASSEMBLY, AND TESTING

Using the dimensions from the analytical model, the two generations of mirror designs are submitted to MUMPS® for fabrication. After fabrication, each mirror is solder assembled using the process described in [3] and then statically tested by measuring the movement of a reflected laser during mirror rotation. Outside of the revised gap height, the changes in the second-generation design are based on experience with the assembly process during assembly of the first-generation design.

Because MUMPS® contains only two releasable polysilicon layers, the lower electrodes are fabricated from the Poly 1 layer and the mirror, flexures, and mirror frame are fabricated from the Poly 2 layer. The mirror is coated with gold using the Metal layer as well. To allow for assembly, each of the three components is only

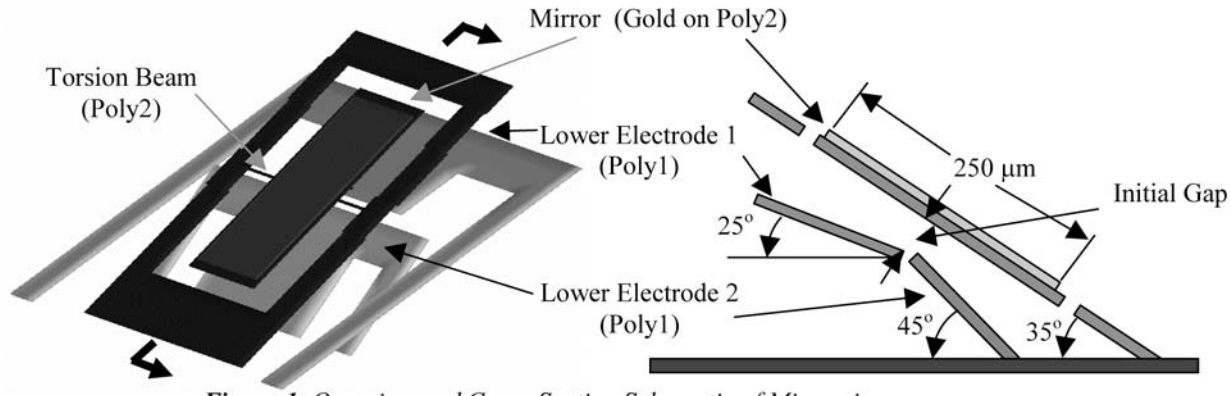

***Figure 1**. Overview and Cross-Section Schematic of Micromirror.*

attached to the substrate with hinge mechanisms at its bottom edge.

Hinge-stops are also included on each component to keep them from rotating too far during assembly. These structures, visible just above the solder balls on the assembled structures in Figures 2 and 3, are T-shaped beams that are hinged to the substrate below each component and then pass through an opening so the top crossbar rests above the component. The crossbar slides down the component face during assembly until it hits a mechanical stop and locks the structure into place. These structures allow for more accurate assembly than solder balls alone could provide [4].

After fabrication, the mirrors are assembled using the process described in [3]. Essentially, solder balls are placed in between two gold pads, one on the rotating component and one fixed to the substrate, on an unreleased device. Then the solder is heated to its melting point. In the presence of Formic Acid, it reacts with the gold and flows out to the edges of the pads. At this point the chip cools and is released normally in Hydrofluoric Acid. Following release, it is again heated in the presence of a gaseous flux, at which time the minimization of surface energy in the solder causes a shape change that assembles the components.

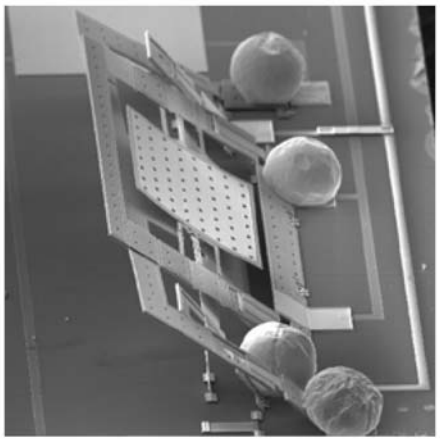

Figure 2. *SEM of First-Generation Device.*

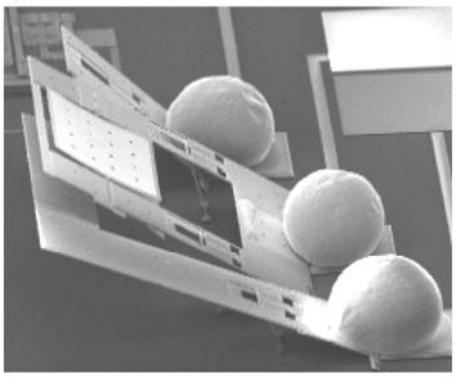

An assembled first-generation mirror is shown in Figure 2 and a second-generation design is shown in Figure 3. These two SEM photographs clearly show the differences between the two generations. The electrode gap in the second-generation design is noticeably larger due to the use of the improved analytical model in the design process. Also the second-generation eliminates the symmetry seen in the first design and uses solder balls that are 8mil in diameter instead of 4mil. The larger solder balls are used for the ease of placement and their seemingly better performance during assembly. As a result of that decision, symmetry is eliminated to keep the overall size of the device in check and to reduce the number of solder balls that need to be placed by 50%.

Finally, samples of the assembled mirrors are statically tested to determine the voltage/angle relationship. The testing is accomplished by reflecting a diode laser beam off the mirror onto an adjacent screen. As the voltage is increased, the movement of the reflected spot is measured and converted into a rotation angle for the mirror. The voltages and rotation angles obtained just before pull-in for three second-generation mirrors are shown in Table 1.

Table 1. *Pull-In Voltages and Angles.*

	Voltage (V)	Angle (°)
Mirror 1	194.2	12.1
Mirror 2	159.0	10.4
Mirror 3	193.3	6.7

DISCUSSION

The data from the static testing is compared with the analytical and FE models to validate model performance. The comparison between the improved analytical model and the first-generation mirror is shown in Figure 4 where the 20% maximum difference between the data and model is reasonable due to variations in material properties and lithography accuracy between MUMPS® fabrication runs. Figure 4 also demonstrates the shortened stable rotation range revealed by the improved model. Instead of ±10° of stable rotation from neutral, only about ±8.7° can be achieved.

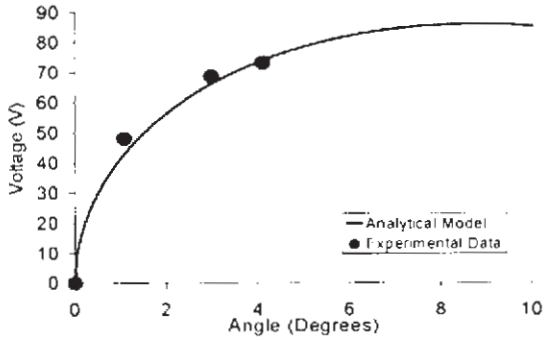

Figure 4. *First-Generation Result Comparison.*

The larger 40 μm gap of the second-generation design succeeds in expanding the stable rotation range as shown in Table 1 and in Figure 5 where the experimental data for three second-generation mirrors as well as the theoretical results from the analytical and FE models are

plotted. Although two of the three mirrors shown in Figure 5 can stably rotate 10° from neutral, the required voltages are lower than those predicted by the improved model, and there is a variation in performance from device to device.

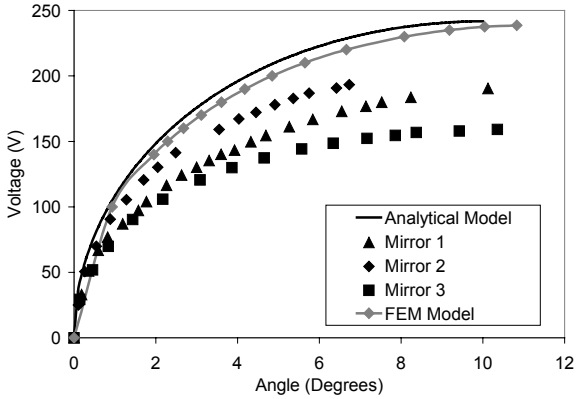

***Figure 5**. Second-Generation Result Comparison.*

The variation between devices is most likely due to the fact that the assembly angles for the mirrors and electrodes are not perfect due to scavenging of the gold pads during the assembly process [3]. Some of the angles are off by as much as 3°. Another factor is variation in mirror warpage between devices. Because the mirrors are only Metal on Poly 2, there is significant warpage that can change with residual stress and temperature variations during assembly. Finally, the assembly force provided by the solder balls can also cause varying degrees of deformation around the gold solder pads. Due to these effects, the initial gap heights differ somewhat from device to device and result in different voltage/angle relationships for each mirror.

The difference between the models and the experimental results can be explained by deformation of the mirror frame and electrode legs. Neither model considers deformation in the electrode and mirror legs. The equations to account for these deformations are not present in the analytical model, and the legs are not included in the FE model. The ends of the torsion beams and the entire lower electrode are fixed. The exclusion of the legs is fine for the first-generation design, as evidenced by Figure 4 because the electrodes are fixed on both sides and the mirror is closer to the substrate. However, the move to the 8mil solder balls requires moving the mirror farther above the substrate and increasing the length of the legs. Thus deformation in the legs is significant in the second-generation design, but not in the first-generation.

In summary, the current work utilizes the beneficial aspects of solder self-assembly to exploit the characteristics of electrostatic parallel-plate actuators. The result is the demonstration of a torsional mirror with a large stable rotation range and a reasonable actuation voltage. These types of devices can be employed in many products such as barcode scanners, optical cross-connects, and free-space communication systems.

ACKNOWLEDGEMENTS

This research is funded by DARPA Grant N66001-00-C-08077. The authors would like to thank Dr. Kevin F. Harsh of the University of Colorado at Boulder for his help with design of the solder assembly mechanism and Dr. Paul E. Kladitis of the Air Force Institute of Technology for his help in refining the solder assembly technique for the mirrors.

REFERENCES

[1] R.R.A. Syms, E.M. Yeatman, "Self-Assembly of Three-Dimensional Microstructures Using Rotation by Surface Tension Forces," *Electron. Lett.*, Vol. 29, No. 9, Apr. 1993, pp. 662-664.

[2] P.W. Green, R.R.A. Syms, "Demonstration of Three-Dimensional Microstructure Self-Assembly," *JMEMSs*, Vol. 4, No. 4, Dec. 1995, pp. 170-176.

[3] K. F. Harsh, V.M. Bright, Y.C. Lee, "Solder Self-Assembly for Three-Dimensional Microelectromechanical Systems," *Sensors and Actuators A: Physical*, Vol. 77, No. 3, Nov. 1999, pp. 237-244.

[4] K.F. Harsh, V.M. Bright, Y.C. Lee, "Design Optimization of Surface Micro-Machined Self-Assembled MEMS Structures," *IPACK'01*, Kaui, Hawaii, July 8-13, 2001.

[5] R.R.A. Syms, "Self-Assembled 3-D Silicon Micro-scanners with Self-Assembled Electrostatic Drives," *IEEE Phot. Tech. Lett.*, Vol. 12, No. 11, Nov. 2000, pp. 1519-1521.

[6] S.S. Lee, L.S. Huang, C.J. Kim, M.C. Wu, "Free-Space Fiber-Optic Switches Based on MEMS Vertical Torsion Mirrors," *J. Lightwave Tech.*, Vol. 17**,** No. 1, Jan. 1999, pp. 7-13.

[7] G.D.J. Su, S.S. Lee, M.C. Wu, "Optical Scanners Realized by Surface-Micromachined Vertical Torsion Mirrors," *IEEE Phot. Tech. Lett.*, Vol. 11, No. 5, May 1999, pp. 587-589.

[8] M.H. Kiang, O. Solgaard, Y.K. Lau, R.S. Muller, "Electrostatic combdrive-actuated micromirrors for laser-beam scanning and positioning," *JMEMS*, Vol. 7, No. 1, Mar. 1998, pp. 27-37.

[9] R.A. Conant, P.M. Hagelin, U. Krishnamoorthy, M. Hart, O. Solgaard, K.Y. Yau, R.S. Muller, "A raster scanning full-motion video display using polysilicon micromachined mirrors," *Sensors and Actuators A: Physical*, Vol. 83, May 2000, pp. 291-196.

[10] http://www.memsrus.com

[11] http://www.coventor.com

[12] http://www.sdrc.com